PAPERS | NOVEMBER 01 2020

Flight and bounce of spinning sports balls

Jacob Emil Mencke; Mirko Salewski ; Ole L. Trinhammer; Andreas T. Adler

Am. J. Phys. 88, 934–947 (2020)
https://doi.org/10.1119/10.0001659

Flight and bounce of spinning sports balls

Jacob Emil Mencke, Mirko Salewski,[a] and Ole L. Trinhammer
Department of Physics, Technical University of Denmark, Fysikvej, 2800 Kgs. Lyngby, Denmark

Andreas T. Adler
Team Danmark, House of Sports, Brøndby Stadion 20, 2605 Brøndby, Denmark

(Received 20 March 2020; accepted 14 July 2020)

Standard university or high-school physics teaching material on projectile motion is usually based on Newton's second law in vacuum, neglecting aerodynamics. We present a low-cost experiment for teaching projectile motion using the students' cell phones and sports equipment, which allows the students to test theory and numerical simulation against experimental data in the real world. For a shot put, theoretical predictions assuming projectile motion in vacuum agree with experimentally obtained trajectories in air to within a few centimeters. However, for a table tennis ball, vacuum trajectories can be almost three times as long as experimentally obtained trajectories. An equation of motion including the aerodynamic drag force has no analytic solution, but it is straightforward to integrate numerically for high-school or first-year university students. Accounting for aerodynamic drag substantially improves the match with experimental data for any ball. In a second experiment, balls are shot with spin resulting in curveball trajectories. Numerical simulations including the Magnus force can give accurate predictions of 3D curveball trajectories, both curving according to the normal and the inverse Magnus effect. Balls shot with topspin and backspin are also accurately modelled. Finally, we model the bounce of an arbitrarily spinning ball using linear and angular impulse-momentum theorems and coefficients of restitution in vertical and horizontal directions. We find agreement with experimental data to within centimeters.
https://doi.org/10.1119/10.0001659

I. INTRODUCTION

Projectile motion in vacuum and collisions between objects are commonly taught in physics classes to high-school and first-year university students.[1] Many of these students are interested if not passionate about sports, which can be used to nurture their interest in physics.[2] Here, we describe a three-day project to study physics of sports balls in the real world, i.e., in air. We determine trajectories of sports balls theoretically and experimentally. In the experiment, we emphasize the use of ordinary cell phone cameras to measure the trajectories and spin rates of sports balls. Experience shows that students are willing to use their own cell phones and sports balls to support this experiment. This ensures that the experiment can be performed at little cost for the university, and the use of their own equipment tends to motivate students, too. Theoretical solutions to the equation of motion from Newton's second law can be calculated analytically (for vacuum) or computationally, i.e., by numerical integration (for air or vacuum). Trajectories of sports balls hence provide a fascinating meeting ground between experimental, theoretical, and computational physics. Our three-day project illustrates how progress in physics can be made by confronting analytically or computationally predicted results with experimental data.

This comparison also quantifies limitations of the commonly taught vacuum assumption in projectile motion theory when applied to sports in the real world. In almost all sports, aerodynamics must be accounted for to explain observed trajectories of sports projectiles.[2] Air resistance decreases the horizontal range, the maximum height, and the time-of-flight of sports balls, often substantially. In many sports, spin is applied to the ball to modify its trajectory. Sidespin generates curveballs, backspin flattens the trajectory and increases the range, and topspin leads to sharply dipping balls with shorter range. Often the best players in sports demonstrate a superior control of the spin of the ball. Due to the importance of ball aerodynamics in many widely popular sports, it comes as no surprise that it has received much attention in recent literature.[3–10]

This paper has three main parts. In Sec. II, we discuss trajectories of balls without spin in vacuum and in air. The analytic vacuum trajectories found in textbooks are reviewed, accounting for the release height of the ball, as the basic, very widespread approximate model to improve upon. We will further discuss how to compute trajectories by numerical integration, which is conceptually simple and can be implemented by high-school or first-year university students. The numerical simulations are discussed for vacuum and for air. We further describe an experimental setup to measure ball trajectories and test the theoretical predictions against experimental data. In Sec. III, we study trajectories of curveballs as well as the effects of topspin and backspin experimentally and theoretically. The spin generates asymmetric flow separation, leading to asymmetric wakes. This deflection of the flow leads to a force on the ball that is perpendicular to the velocity and the spin vector. Despite the complex fluid mechanical phenomenology, the trajectories of curveballs as well as of balls launched with topspin or backspin can be calculated accurately. In Sec. IV, we discuss bouncing of arbitrarily spinning balls, which completes the analysis of the most important elements of sports ball motion. The bounce of a ball can be described by an algebraic set of equations derived from the linear and angular impulse-momentum theorems. These bounce equations are also appropriate for courses for first-year university students and may even be applied in upper level high school. Section V concludes the paper.

II. TRAJECTORIES OF BALLS WITHOUT SPIN IN VACUUM AND IN AIR

In this section, we study trajectories of balls without spin, first in vacuum, neglecting aerodynamics, and then in air. The trajectory of a projectile with mass m is given by Newton's second law,

$$m\mathbf{a} = \mathbf{F}, \tag{1}$$

where $\mathbf{a}$ is the acceleration vector of the ball and $\mathbf{F}$ is a vector describing the forces on the ball. In a Cartesian 3D coordinate system (x, y, z), we write an equation for each component.[1] For example, for the x-component,

$$ma_x = F_x. \tag{2}$$

The acceleration is the derivative of the velocity, which in turn is the derivative of the position,

$$a_x = \frac{dv_x}{dt}, \tag{3}$$

$$v_x = \frac{dx_x}{dt}. \tag{4}$$

The y- and z-components are analogous.

A. Projectile motion in vacuum

In vacuum, the only force acting on a ball or in fact any arbitrarily shaped and spinning projectile is gravity which acts in the negative y-direction in our coordinate system. Alan Shepard hit two golf balls on the moon towards the end of the 1971 Apollo 14 mission.[11] This is probably one of the few, if not the only, examples where a sport is played in vacuum. As we will quantify below, the vacuum trajectory will be a good approximation for heavy, small objects at low speed, e.g., a shot put. The vacuum trajectory can be determined analytically, i.e., by analytic integration, or numerically, i.e., by numerical integration. This vacuum trajectory matches an experimentally determined trajectory in air to within a few centimeters for a shot put. The only non-zero force in vacuum is $F_y = -mg$ in Eq. (1), which gives the acceleration using Newton's second law, $a_y = -g$.[12,13]

1. Analytic solution

The analytic vacuum solution of projectile motion is discussed in many basic physics textbooks.[12,13] Integrating the accelerations twice over time gives the position of the ball,

$$x = v_{x0}t + x_0, \tag{5}$$

$$y = -\frac{1}{2}gt^2 + v_{y0}t + y_0, \tag{6}$$

$$z = v_{z0}t + z_0. \tag{7}$$

The integration constants $x_0, y_0, z_0, v_{x0}, v_{y0}$, and v_{z0} are the initial conditions of the ball right after the launch, which can be seen by setting $t = 0$. Without loss of generality, we now place the origin of our coordinate system right below the initial position of the ball, so that $x_0 = z_0 = 0$. However, sports projectiles are often released from a height $y_0 > 0$ above the ground, which we, therefore, do not set to zero. Furthermore, we turn our coordinate system such that the ball has $v_{z0} = 0$. In these coordinates and without aerodynamics, $z = 0$ at all times t, and we can conveniently describe the motion in just two coordinates (see Fig. 1).

The initial velocity can be described in polar coordinates,

$$v_{x0} = v_0 \cos(\theta_0), \tag{8}$$

$$v_{y0} = v_0 \sin(\theta_0). \tag{9}$$

v_0 is the speed, and θ_0 is the launch angle with respect to the horizontal. We then obtain the simpler, but completely general set of equations describing the trajectory,[12,13]

$$x = v_0 \cos(\theta_0)t, \tag{10}$$

$$y = -\frac{1}{2}gt^2 + v_0 \sin(\theta_0)t + y_0, \tag{11}$$

$$z = 0. \tag{12}$$

Elimination of t explicitly shows that the trajectory in vacuum is a parabola,[12,13]

$$y = -\frac{g}{2v_0^2 \cos^2(\theta_0)}x^2 + \tan(\theta_0)x + y_0. \tag{13}$$

Characteristic parameters describing this motion are the time-of-flight T, the horizontal range X, and the maximum height Y. The time-of-flight is found by setting $y = 0$ in Eq. (11), which has a solution at $t \leq 0$ (before or at the launch) and one at $t > 0$ which is the time-of-flight T. The horizontal range is given by $X = v_{x0}T$. The maximum height is found by the condition $(dy/dt) = 0$ in Eq. (11) which gives the time at which the maximum height is achieved and which is substituted into Eq. (11). Hence, the time-of-flight T, the horizontal range X, and the maximum height Y are, respectively,[2,14,15]

$$T = \frac{v_0 \sin(\theta_0)}{g}\left(1 + \sqrt{1 + \frac{2gy_0}{v_0^2 \sin^2(\theta_0)}}\right), \tag{14}$$

$$X = \frac{v_0^2 \sin(2\theta_0)}{2g}\left(1 + \sqrt{1 + \frac{2gy_0}{v_0^2 \sin^2(\theta_0)}}\right), \tag{15}$$

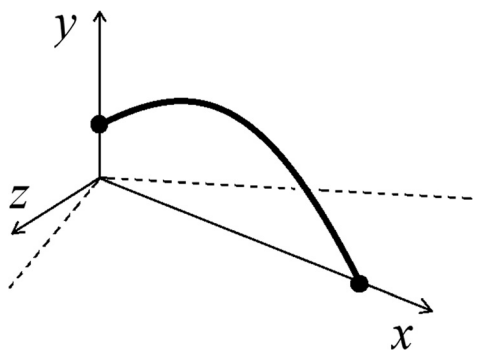

Fig. 1. A possible trajectory for a shot put. We rotate the coordinate system to have $z = 0$ throughout the trajectory. Note that the initial height y_0 is different from zero.

$$Y = \frac{v_0^2 \sin^2(\theta_0)}{2g} + y_0. \tag{16}$$

We have used that $\sin(2\theta_0) = 2\sin(\theta_0)\cos(\theta_0)$. Setting $y_0 = 0$ gives the perhaps more familiar ground-launch equations for the time-of-flight, the horizontal range and the maximum height (the brackets become a factor two).[12,13] The analytic computation of these parameters are part of many basic physics classes for first-year university students. The ground-launch range is maximized for $\theta_0 = 45°$, where $\sin(2\theta_0) = 1$. However, the optimal release angle for maximum range is lower than 45° if the ball is released at a height y_0 (in vacuum). It is found by differentiating X with respect to θ_0. The result is[15]

$$\theta_{\mathrm{Xmax}} = \arcsin \frac{1}{\sqrt{2\left(1 + \frac{y_0 g}{v_0^2}\right)}}. \tag{17}$$

The higher the release height, the lower the optimum launch angle for a given speed. However, we should note that for a given power of a particular athlete, y_0 and v_0 are usually related. For example, the lower the launch angle in a shot put is, the higher the release speed of the shot put is for a given power of the athlete. Energetically, the given power of an athlete is used to increase both the potential and the kinetic energy during the put.[14] A larger release angle requires the projectile to have more potential energy at the launch for a given arm length of an athlete, so that less power is available to increase the kinetic energy of the projectile. Therefore, Eq. (17) is not applicable to calculate the optimum release angle in a shot put.

2. Numerical solution

The vacuum trajectory can alternatively be computed by numerical integration instead of analytic integration. A comparison of analytically and numerically computed trajectories is useful to validate the numerical code, before aerodynamic effects are taken into account. Such a comparison is only possible for vacuum as no general analytic solution for ball motion in air is known. MATLAB and PYTHON codes are provided in the supplementary material.[32] In the simplest numerical solution, the first step is to approximate the derivatives by first-order forward finite differences,[1]

$$a_x(t) \approx \frac{v_x(t + \Delta t) - v_x(t)}{\Delta t}, \tag{18}$$

$$v_x(t) \approx \frac{x(t + \Delta t) - x(t)}{\Delta t}. \tag{19}$$

Given the position, velocity, and acceleration at a time t, we can compute the position and velocity a little time Δt later,[1]

$$v_x(t + \Delta t) \approx v_x(t) + a_x(t)\Delta t, \tag{20}$$

$$x(t + \Delta t) \approx x(t) + v_x(t)\Delta t. \tag{21}$$

The y- and z-components are analogous. As we know the initial conditions, we can calculate an approximate trajectory by this numerical integration. This is known as the Euler method.

For motion in vacuum, the only non-zero acceleration is $a_y = -g$. For motion of non-spinning and spinning balls in air, the accelerations will be described in Secs. II B and III, respectively. For $\Delta t \to 0$, the exact derivative is recovered, and hence, the trajectory approaches the analytic solution, but the computation takes increasingly longer time for shorter step sizes. To estimate the required size of the time step Δt, we compare the numerically and analytically computed solutions of the trajectory for various time step sizes (Fig. 2). For about 10 ms time steps, we get an accurate result for a soccer ball released at 40 m/s at 45°. More sophisticated numerical integration schemes, e.g., a fourth-order Runge-Kutta scheme available in MATLAB or PYTHON, will often be more efficient to calculate accurate trajectories. Nevertheless, we stress that even the conceptually simple Euler method yields accurate results as long as we choose the time step small enough, which is a clear advantage when teaching students.

B. Projectile motion in air

In the real world, balls move in air and are slowed down by air drag,[2,16,17]

$$\mathbf{F}_{\mathrm{D}} = -\frac{1}{2} c_{\mathrm{D}} \pi R^2 \varrho |\mathbf{v} - \mathbf{v}_{\mathrm{w}}| (\mathbf{v} - \mathbf{v}_{\mathrm{w}}). \tag{22}$$

$\mathbf{v}$ and $\mathbf{v}_{\mathrm{w}}$ are the velocities of the ball and the wind with respect to a stationary observer, respectively. c_{D} is the drag coefficient of the ball, R is the radius of the ball, and ϱ is the air density. This vector equation shows that the air drag always goes in the direction against the aerodynamic velocity $\mathbf{v} - \mathbf{v}_w$. The drag coefficient depends on the Reynolds numbers Re, the spin, and the surface of the ball. For a soccer ball without spin, one can take the empirical model,[5]

$$c_{\mathrm{D}} = 0.155 + 0.346 \Big/ \left(1 + \exp\left(\frac{v - v_{\mathrm{c}}}{v_{\mathrm{s}}}\right)\right), \tag{23}$$

where $v_{\mathrm{c}} = 12.19$ m/s and $v_{\mathrm{s}} = 1.309$ m/s. This model does well in reproducing the drag reduction when the boundary layer around a soccer ball becomes turbulent. This transition from laminar to turbulent boundary layer flow happens for velocities around v_c over a velocity interval width that is related to v_s. However, other empirical models may do equally well or better.[3,4,18–20] It is useful to formulate Eq. (23) in terms of the Reynolds number (in terms of the diameter of the ball, $D = 2R$),

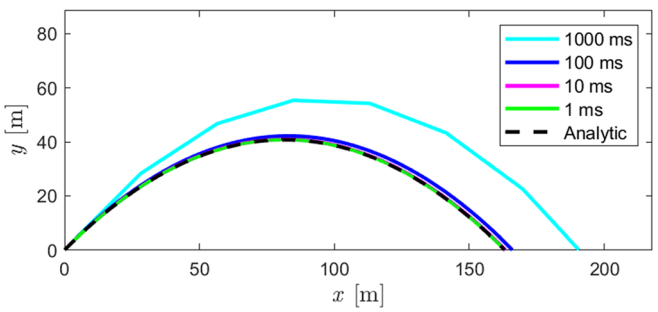

Fig. 2. Comparison of numerically simulated and analytic soccer ball trajectories in vacuum for various time step sizes Δt in (ms). $\theta_0 = 45°$. $v_0 = 40$ m/s. For $\Delta t = 1$ ms or 10 ms, the numerical solutions are within centimeters of the analytic vacuum solution.

$$\mathrm{Re} = \frac{vD}{\nu}, \tag{24}$$

where ν is the kinematic viscosity of air. The Reynolds number is a similarity parameter which describes the ratio of inertial and viscous forces in flows.[6] Incompressible flows (i.e., low Mach number flows) with the same Reynolds number and the same boundary conditions are identical. For example, if the diameter of a ball is doubled and the flow speed is halved, the Reynolds number and, hence, the flow will be the same. In terms of the Reynolds number, we get

$$c_\mathrm{D} = 0.155 + 0.346 \Big/ \left(1 + \exp\left(\frac{\mathrm{Re} - \mathrm{Re_c}}{\mathrm{Re_s}}\right)\right), \tag{25}$$

where the Reynolds numbers $\mathrm{Re_c}$ and $\mathrm{Re_s}$ are computed using v_c and v_s. The dependence of the drag coefficient on the Reynolds number is illustrated in Fig. 3. The strong decrease in c_D for increasing Reynolds number near the critical Reynolds number is referred to as the drag crisis. For $\mathrm{Re} < \mathrm{Re_c}$, the boundary layer is laminar; and for $\mathrm{Re} > \mathrm{Re_c}$, it becomes turbulent. The drag crisis appears because flow with a turbulent boundary layer stays attached to the ball for longer than a laminar boundary layer in the rear region of the ball, where there is an adverse pressure gradient until the flow separates from the ball.[6,27] After the flow separation point, there is a low pressure region in the wake of the ball, and this low pressure region is smaller in the case of a turbulent boundary layer. Therefore, the drag coefficient becomes smaller when the boundary layer becomes turbulent. Sports balls are designed to promote transition from laminar to turbulent flow in the boundary layer by roughness elements. For example, golf balls have dimples, tennis balls have fuzz, and soccer balls and volleyballs have some kind of pattern that changes from design to design. These roughness elements trip the boundary layers close to the ball surface to become turbulent all around the ball. In terms of Eqs. (23) and (25), the surface roughness lowers v_c and $\mathrm{Re_c}$, so that the balls are usually played in the low c_D region.

Gravity and drag are the dominant forces on balls without spin in most sports, and we will neglect other forces. Sometimes buoyancy, which is the force on a body immersed in a fluid (air or water), may be important. Buoyancy is directed opposite to gravity,[12,13]

$$\mathbf{F}_\mathrm{B} = -\varrho V \mathbf{g} = -\frac{4}{3}\pi R^3 \varrho \mathbf{g}, \tag{26}$$

where V is the volume of the ball so that ϱV is the mass of the displaced fluid. Other fluid mechanical forces on balls can be estimated to be small: the Faxen force, forces due to flow acceleration, the added mass force, and the Basset history force.[16,21,22] Accounting for air drag but not the other forces, Newton's second law is

$$m\mathbf{a} = \mathbf{F}_\mathrm{g} + \mathbf{F}_\mathrm{D}. \tag{27}$$

The accelerations in the three directions are, hence,

$$a_x = -\frac{1}{2m} c_\mathrm{D} \pi R^2 \varrho |\mathbf{v} - \mathbf{v}_\mathrm{w}| (v_x - v_{\mathrm{w},x}), \tag{28}$$

$$a_y = -g - \frac{1}{2m} c_\mathrm{D} \pi R^2 \varrho |\mathbf{v} - \mathbf{v}_\mathrm{w}| (v_y - v_{\mathrm{w},y}), \tag{29}$$

$$a_z = -\frac{1}{2m} c_\mathrm{D} \pi R^2 \varrho |\mathbf{v} - \mathbf{v}_\mathrm{w}| (v_z - v_{\mathrm{w},z}). \tag{30}$$

Note that

$$|\mathbf{v} - \mathbf{v}_\mathrm{w}| = \sqrt{(v_x - v_{w,x})^2 + (v_y - v_{w,y})^2 + (v_z - v_{w,z})^2} \tag{31}$$

is shorthand for a scalar. The equations of motion cannot be integrated analytically, but they can easily be integrated numerically. Codes solving these equations are provided in the supplementary material.[32]

By dimensional analysis, we can see that the quantity

$$\tau = \frac{2m}{c_\mathrm{D} \pi R^2 \varrho |\mathbf{v} - \mathbf{v}_\mathrm{w}|} \tag{32}$$

is a characteristic time scale of balls in flight. It indicates how quickly balls approach the wind speed in x and z-directions (or decelerate, if there is no wind).[17] Light, large balls with large drag coefficients in dense air are fastest to react. Further insight can be gained by non-dimensionalizing the equation of motion using the ball radius R as characteristic length scale and the launch speed v_0 as characteristic velocity scale.[6] The characteristic time scale is then R/v_0 rather than τ. The time scale R/v_0 shows how quickly a ball moves a distance of one ball radius. The dimensionless variables are

$$\hat{x} = x/R, \tag{33}$$

$$\hat{v} = v/v_0, \tag{34}$$

$$\hat{t} = tv_0/R. \tag{35}$$

Introducing $x = \hat{x}R$, $v = \hat{v}v_0$, and $t = \hat{t}R/v_0$ into Eq. (27) and dividing by mg gives a dimensionless equation of motion,

$$A\frac{d^2\hat{\mathbf{x}}}{d\hat{t}^2} = -\mathbf{e}_y - \frac{1}{B}|\hat{\mathbf{v}} - \hat{\mathbf{v}}_\mathrm{w}|(\hat{\mathbf{v}} - \hat{\mathbf{v}}_\mathrm{w}). \tag{36}$$

$\mathbf{e}_y$ is the unit vector in the y-direction. Two dimensionless groups appear[6]

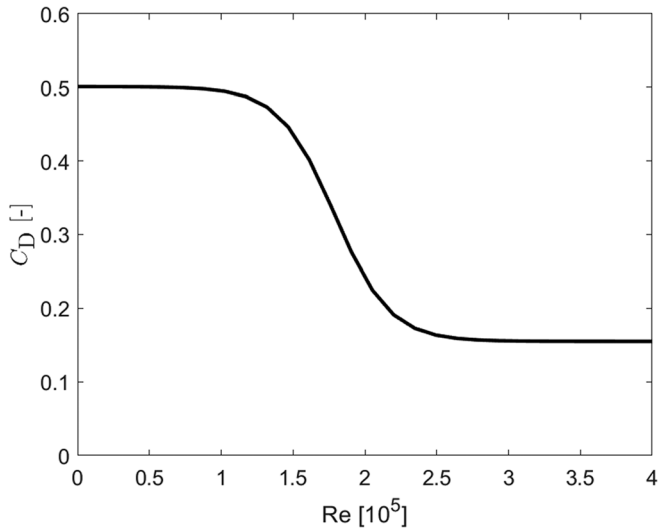

Fig. 3. Drag coefficient as a function of Reynolds number Re.

$$A = \frac{v_0^2}{Rg}, \tag{37}$$

$$B = \frac{mg}{\frac{1}{2} c_D \pi R^2 \varrho v_0^2}. \tag{38}$$

A is the range parameter which shows the maximum possible range in vacuum normalized to the ball radius [see Eq. (15)]. B is the ballistic parameter which is the ratio of the gravitational force and the drag force. (The definition of B in Ref. 6 is different by $c_D/2$.) Two balls with the same parameters A and B and the same dimensionless initial conditions have the same solution in dimensionless variables $\hat{\mathbf{x}}$ and $\hat{t}$. Note, however, that B depends on c_D which in turn depends on the surface roughness and the Reynolds number. Nevertheless, the dimensionless parameters provide useful insight. If $B \gg 1$, the drag force is not important. If $B \ll 1$, gravity is much smaller than drag. Figure 4 illustrates different ball trajectories of soccer balls launched at 10, 20, 30 and 40 m/s in air and in vacuum. The parameters A and B for these launch speeds are summarized in Table I. The range parameter A ranges from about 90 to 1500. The ballistic parameter ranges from $B = 0.77$ for the longest trajectory launched at 40 m/s to $B = 12$ for the shortest trajectory launched at 10 m/s. 40 m/s is a large speed for a soccer ball that is achievable by powerful athletes. Aerodynamic drag reduces the range of such a shot almost by a factor of two, from about 160 m in vacuum to 80 m in air.

C. Experimental setup for trajectory measurements

To confront projectile motion theory and numerical simulations with experimental data, we must determine ball trajectories experimentally. Here, we describe an experimental setup using the students' cell phones and sports balls. We will focus on trajectories of a shot put, a table tennis ball, and a soccer ball. The experimental data can be acquired as follows: One student launches the ball, and another student films the entire trajectory of the ball from the side with a cell phone. It is helpful if a third student films the launch of the ball in close-up to capture the launch velocity and possibly the spin vector. This provides a high-resolution measurement of the initial conditions of the ball right after the kick. Nevertheless, the initial conditions can also be retrieved from the other camera dedicated to the whole trajectory. If a 3D trajectory is required, e.g., due to wind or an oblique launch of the ball with respect to the projected plane seen by the camera, a fourth student can film the trajectory from the front. The arrangement of cameras is illustrated in Fig. 5.

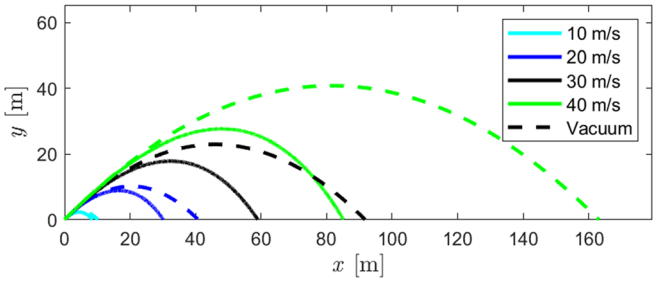

Fig. 4. Comparison of simulated soccer ball trajectories in vacuum and in air. Launch angle $\theta_0 = 45°$. Launch speed: 10, 20, 30, and 40 m/s. The dashed lines are vacuum trajectories, and the full lines account for air drag.

Table I. Range and ballistic parameters A and B for soccer ball kicks with different launch speeds. $R = 0.11$ m, $\varrho = 1.2$ kg/m^3, and $m = 0.43$ kg.

v_0 (m/s)	A	B
10	93	12
20	371	3.1
30	834	1.4
40	1480	0.77

It is easy to synchronize the movies by using the kick as common reference point. We found that sometimes the frame rate of cell phones can deviate from their nominal frame rate. The frame rate can be established by filming a stopwatch. One or several scale sticks (or a soccer goal of known dimensions) help to set the scale of the movie. The movies can be processed with standard tracking software such as the freely available software TRACKER.

The trajectories of several different projectiles could be compared with the corresponding ideal vacuum trajectories. Inexpensive examples are a shot put as an extreme following the vacuum trajectory well and a shuttlecock or table tennis ball which do not follow the vacuum trajectory well at all. At European universities, it is highly popular to study trajectories of soccer balls. A comparison of a golf ball and a table tennis ball, which have similar radii but different masses, is also instructive.

D. Comparisons of theoretical and measured trajectories for balls without spin

Figure 6 shows a comparison of a measured trajectory of a shot put with numerically simulated trajectories in air and in vacuum as well as the analytic vacuum trajectory. The put has been made by a trained athlete as can be seen from the fairly large range of the shot put (>15 m). As the athlete was fairly tall, the launch height was more than 2 m. The initial velocities for the shot put and the other trajectories that we consider here are summarized in Table II. The time step of the numerical integration is selected small enough that the analytically and numerically computed parabolic vacuum trajectories are almost identical. The computed trajectory accounting for air drag is also almost identical to the vacuum trajectories (∼5 cm shorter). The measured trajectory matches the simulated trajectory with air drag best, but the vacuum trajectories are also within centimeters. We can conclude that all four curves are almost identical for a shot put. This is not surprising because the aerodynamic forces on a shot put are insignificant compared to the gravitational force.

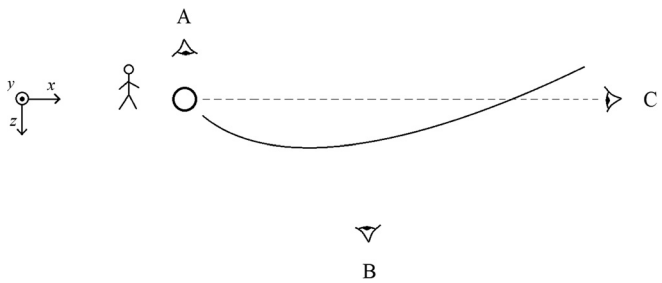

Fig. 5. Illustration of the experimental setup for trajectory measurements. Camera A films the ball launch in close-up, camera B captures the motion in the (x, y)-plane, and camera C captures the motion in the (y, z)-plane.

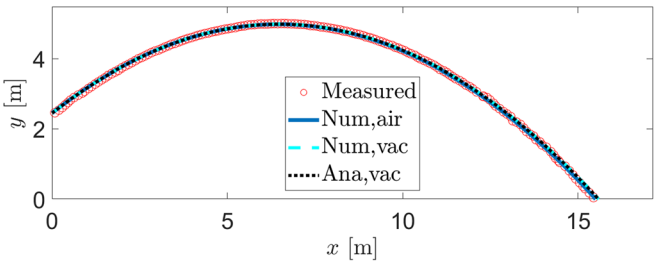

Fig. 6. Trajectory of a shot put. Numerical and analytic vacuum solutions and numerical solution including air resistance, all compared to a measurement of the trajectory.

Due to the large mass of 7.26 kg, the ballistic parameter becomes very large ($B \sim 530$).

The situation changes dramatically when we measure and calculate trajectories of soccer balls or table tennis balls (Fig. 7). In each case, the measured trajectories are now substantially lower and shorter than the corresponding vacuum solutions. The analytic and simulated vacuum solutions are almost identical for this case which indicates that the time step is chosen small enough. We only plot the analytic vacuum solution. However, both for the soccer ball and the table tennis ball, the simulated trajectories accounting for air drag match the measured trajectories well. For the soccer ball, the ballistic parameter for this shot is $B = 5.5$ which means that the gravitational force is about 5.5 times larger than the aerodynamic force right after the launch. For the table tennis ball, $B = 0.83$ which means that the aerodynamic drag force is even larger than the gravitational force right after the launch. For such ballistic parameters, the trajectories of balls in air deviate substantially from the vacuum trajectories. This shows that air drag must be accounted for to accurately predict the motion of a soccer ball or a table tennis ball, or other balls with similar ballistic parameters. We further observe a clear asymmetry in the measured and simulated trajectories accounting for air drag. Whereas the ascending part of the trajectory is almost perfectly mirror symmetric to the descending part for the shot put, the descending part of the trajectory is substantially shorter for soccer balls and table tennis balls.[2]

III. TRAJECTORIES OF SPINNING BALLS

In this section, we compare measured trajectories of spinning balls with simulations. Spin modifies the trajectory of balls due to an additional force on the ball which is called the Magnus force. We focus on curveballs for a soccer ball and for a smooth plastic ball with sidespin where the Magnus force is the dominant sideways force. Sideways forces can also be generated by asymmetries in geometry or surface properties of spin-stabilized balls, rather than the Magnus force itself.[3,4] We will not study such effects here.

Table II. Initial conditions and dimensionless parameters A and B of a shot put, a soccer ball, and a table tennis ball.

	v_{x0} (m/s)	v_{y0} (m/s)	A	B
Shot put	9.0	7.1	220	530
Soccer ball	11.0	10.2	210	5.5
Table tennis ball	11.8	12.0	1400	0.83

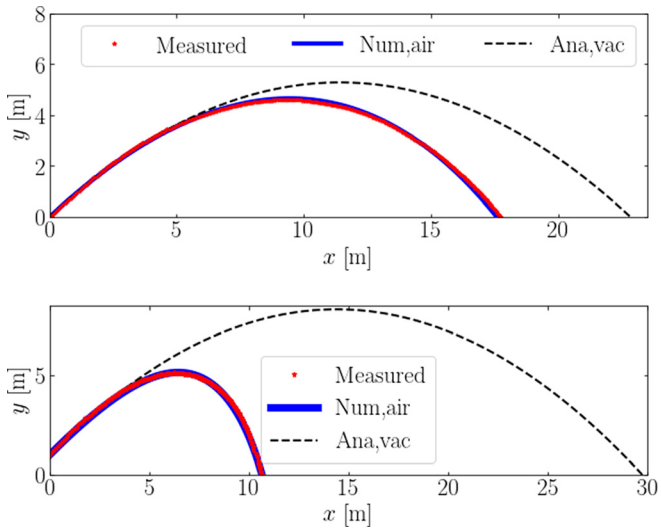

Fig. 7. Trajectories of a soccer ball (upper graph) and a table tennis ball (lower graph). Analytic vacuum solution, numerical solution including air resistance, and measurement of the trajectory.

The effects of topspin and backspin are more difficult to observe. We will study topspin and backspin of a volleyball delivered by a ball launch machine at various spin rates.

A. Drag and Magnus force on spinning balls

The Magnus force is a force due to spin of the ball. It is perpendicular to the aerodynamic velocity $(\mathbf{v} - \mathbf{v}_w)$ and to the spin vector $\boldsymbol{\omega}$ (rad/s),

$$\mathbf{F}_M = c_L \pi R^3 \varrho \boldsymbol{\omega} \times (\mathbf{v} - \mathbf{v}_w), \tag{39}$$

where c_L is the lift coefficient.[6] We assume that the spin vector is constant during the flight of the ball which appears to be a reasonable approximation. The spin vector of a ball will be almost constant if the transfer of angular momentum from the ball to air is slow. The direction of the spin vector is defined by the right hand rule: If the fingers follow the direction of the spin, the thumb will define the direction of the spin vector. As the Magnus force is perpendicular to the aerodynamic velocity, it is referred to as a lift force in analogy to aircraft aerodynamics. However, the Magnus force can act in any direction perpendicular to the velocity vector, depending on the direction of the spin vector. In vector form, Newton's second law including the Magnus force, drag, and gravity is

$$m\mathbf{a} = \mathbf{F}_g + \mathbf{F}_D + \mathbf{F}_M. \tag{40}$$

The components of the spin vector in (x, y, z) are $(\omega_x, \omega_y, \omega_z)$. The accelerations are

$$a_x = -\frac{1}{2m} c_D \pi R^2 \varrho |\mathbf{v} - \mathbf{v}_w| (v_x - v_{w,x}) + \frac{1}{m} c_L \pi R^3 \varrho \left(\omega_y (v_z - v_{w,z}) - \omega_z (v_y - v_{w,y})\right), \tag{41}$$

$$a_y = -g - \frac{1}{2m} c_D \pi R^2 \varrho |\mathbf{v} - \mathbf{v}_w| (v_y - v_{w,y}) + \frac{1}{m} c_L \pi R^3 \varrho \left(\omega_z (v_x - v_{w,x}) - \omega_x (v_z - v_{w,z})\right), \tag{42}$$

$$a_z = -\frac{1}{2m} c_D \pi R^2 \varrho |\mathbf{v} - \mathbf{v}_w| (v_z - v_{w,z}) + \frac{1}{m} c_L \pi R^3 \varrho \left(\omega_x (v_y - v_{w,y}) - \omega_y (v_x - v_{w,x})\right). \quad (43)$$

The equations of motion can be integrated numerically. Codes solving these equations are provided in the supplementary material.[32] As for balls without spin, it is useful to non-dimensionalize the equation of motion,[6]

$$A \frac{d^2 \hat{\mathbf{x}}}{d\hat{t}^2} = -\mathbf{e}_y - \frac{1}{B} |\hat{\mathbf{v}} - \hat{\mathbf{v}}_w| (\hat{\mathbf{v}} - \hat{\mathbf{v}}_w) + \frac{2c_L}{c_D} \frac{S}{B} \hat{\boldsymbol{\omega}}_e \times (\hat{\mathbf{v}} - \hat{\mathbf{v}}_w) \quad (44)$$

where the normalization is executed in the same way as for Eq. (36) and $S\hat{\boldsymbol{\omega}}_e = \boldsymbol{\omega} R / v_0$. Here, the dimensionless spin vector is written as a product of the spin parameter S and the unit (dimensionless) spin vector $\hat{\boldsymbol{\omega}}_e$. The spin parameter S is given by

$$S = \frac{\omega R}{v_0}. \quad (45)$$

It is related to the ratio of the Magnus force and the drag force,

$$\frac{F_M}{F_D} = \frac{2c_L}{c_D} S, \quad (46)$$

for $\hat{\mathbf{v}}_w = 0$. In addition to the spin parameter, the Magnus term has the inverse of the ballistic parameter B as a factor and hence becomes unimportant for large B.

Experiments show that the drag on a spinning ball also depends on the spin rate. Accounting for spin, the drag model can be extended as follows:[5] If $S > 0.05$ and $v > v_c$, use

$$c_D = 0.4127 \times S^{0.3056}, \quad (47)$$

or else use Eq. (23). The lift coefficient c_L is of order unity, but can actually also be negative, e.g., for ordinary plastic balls for children. One may set for a plastic ball $c_L = -0.7$ and for a soccer ball $c_L = 0.9$. These values can be determined by fitting simulated trajectories to an experimentally measured trajectory. The Magnus force can easily be larger than the drag force and the gravitational force in many sports (table tennis, soccer, tennis, and volleyball).[7]

Finally, we study the generation of spin during a kick from rest. The ball needs to be hit off center at a fraction $\epsilon \in [0; 1]$ of the radius R of the ball. Then, the spin parameter is bounded by a theoretical maximum assuming stiff bodies and no slip between the ball and the foot during the kick. From linear and angular impulse-momentum theorems follow [see Eq. (53) in Sec. III B]

$$\epsilon R m v = \alpha m R^2 \omega, \quad (48)$$

which implies that the maximum achievable spin parameter for an off-center hit at a fraction ϵ of the radius of the ball is

$$S_{max} = \frac{\omega R}{v} = \frac{\epsilon}{\alpha}, \quad (49)$$

where $\alpha = 2/3$ for hollow balls [see Eq. (52)]. Practically observed spin parameters in sports are well below one.

B. Magnus effect and inverse Magnus effect

Spinning sports balls will curve in the direction of $\boldsymbol{\omega} \times \mathbf{v}$ as modeled by the Magnus force term without wind. However, a highly interesting and puzzling effect appears for spinning balls which are close to the critical Reynolds number. For example, many smooth spinning plastic balls for children will curve in the direction of $-\boldsymbol{\omega} \times \mathbf{v}$. The force causing curvature in "the wrong direction" is often referred to as the inverse Magnus force.

As described in Sec. II, sports balls are designed to promote the transition from laminar flow to turbulent flow in the boundary layer close to the ball by roughness elements. The balls are played well above the critical Reynolds number. In the case of turbulent boundary layers everywhere (well above Re_c), the flow will separate from the surface at an earlier point on the side of the ball with the larger relative velocity between the flow and the local surface of the ball. The wake is therefore deflected to that side. The deflection of the flow leads to a deflection of the ball in the opposite direction. This effect is referred to as the Magnus effect and is described by the Magnus force. The asymmetric flow separation explaining the Magnus effect is illustrated in Fig. 8.

However, smooth balls do not promote the transition from laminar to turbulent boundary layer flow. In some speed and spin ranges, such balls can therefore have laminar flow on

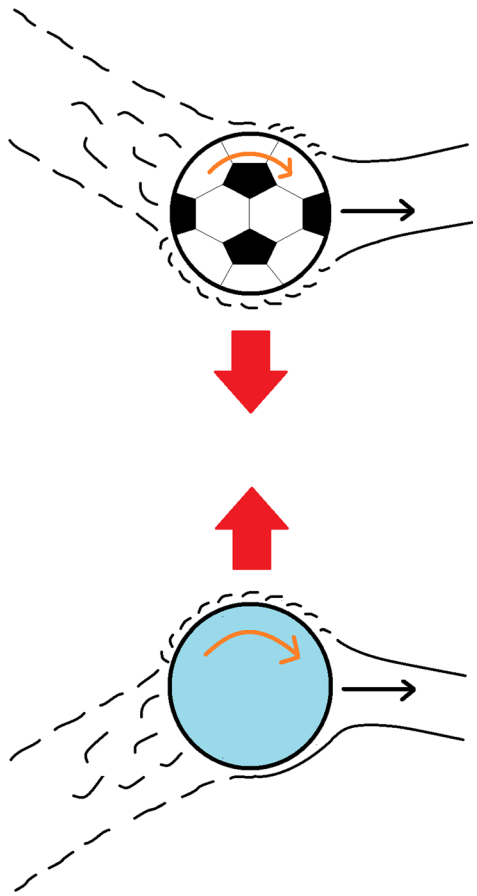

Fig. 8. Illustration of boundary layers and asymmetric wakes for the Magnus effect and the inverse Magnus effect. The black arrows indicate the ball velocity, the curved arrows the spin direction, and the red arrows the force on the ball. The boundary layers of the football and the top boundary layer of the plastic ball are turbulent, whereas the bottom boundary layer of the plastic ball is laminar.

the side with low relative velocity between the air and the local velocity of the surface and turbulent flow on the side with large relative velocity (in the vicinity of Re_c). In that case, the flow will separate earlier on the laminar flow side, i.e., now on the side with smaller relative velocity. This phenomenon is referred to as the inverse Magnus effect because such a ball curves "the wrong way" compared to what we are used to from properly designed sports balls. The asymmetric flow separation explaining the inverse Magnus effect is illustrated in Fig. 8. Beautiful flow visualization photographs capturing the Magnus effect and the inverse Magnus effect are presented in Ref. 23.

The Magnus force as well as the inverse Magnus force can be understood by considering the conservation of momentum using the control volume illustrated in Fig. 9. The most intuitive control volume is thin in the flight direction and very long in the direction of the Magnus force.[25] In such a control volume, the integrated pressures on the narrow upper and lower sides are approximately equal, such that the integrated sideways momentum flux of the flow entering and exiting the control volume in the front and the rear of the ball is equal and opposite to the Magnus force. Note that the flow entering the control volume has sideways momentum in the same direction as the Magnus force, and the flow exiting the control volume has sideways momentum in the direction opposite to the Magnus force as illustrated in Fig. 8. Similar lifting flows have been described in the context of aircraft.[24] For shorter control volumes in the sideways direction, the asymmetric pressure field on the upper and lower sides of the control volume must also be considered in the momentum balance[25] (pressure can be understood as momentum flux normal to the surface).

Sometimes the nature of curveballs is simplistically explained by pointing to a speeding up of the air on one side and a slowing down of the air on the other side and then appealing to Bernoulli's equation to argue for a pressure change.[12,13,26] However, this type of explanation cannot explain the appearance of an inverse Magnus effect in which the ball curves the wrong way for the same spin.[27] A fundamental flaw in this type of explanation, which often neglects the asymmetric flow separation, is that the motion of the ball surface is ultimately argued to be responsible for speeding up or slowing down of the flow. However, the motion of the surface can only have an impact on the flow through viscous or turbulent shear stresses. The presence of shear stresses violates the premises for Bernoulli's equation, and so, it cannot be applied to explain the Magnus effect.

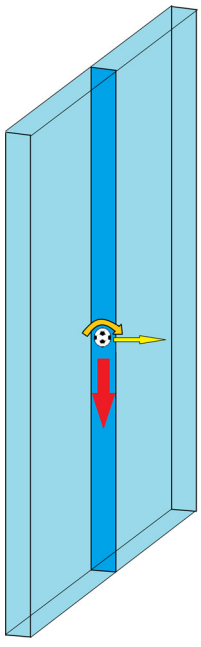

Fig. 9. Control volume used to illustrate the conservation of momentum for a ball subject to the Magnus force. The large distances to the lateral control surfaces make pressure differences negligible (Ref. 25).

C. Experimental setup for spinning balls

The experimental setup is very similar to the setup used to study balls without spin. Whereas the trajectories of balls without spin can be measured well experimentally by just one camera, two cameras are necessary to measure the 3D trajectories of curveballs. Often a close-up movie with a third camera is helpful to get a good measurement of the spin of the ball in addition to its launch velocity vector (see Fig. 5). As already mentioned, we will assume the spin vector to be constant during the flight of the ball, which will give accurate results for the trajectory. The decay of spin is discussed in Ref. 10. Whereas high frame rates are not necessary to capture the trajectories of sports balls, the spin of a ball is often difficult to capture with standard frame rates. Frame rates of more than 100 frames per second are often advisable to get a good measurement of the spin rate. Most modern cell phones from about 2015 can record at such frame rates, the newest models even higher (~400 frames per second). For movies recorded with cell phones at such high frame rates, the environment must have a lot of light, e.g., bright sunlight. If the ball has no visible patterns (table tennis, tennis), one can draw a pattern on the ball to allow observation of the spin.

Movies from the front or the back can demonstrate the trajectory of a curveball on film convincingly (see Fig. 5). It is beneficial if the ball crosses the path from the shooter to the camera, so that the ball in the movie first moves to one side, then to the other side. This change of sideways direction of motion is characteristic for a curveball. Such a camera positioning is used in Sec. III D, where the camera tracking the sideways motion is at $z = 0$. Wind can hamper a clear demonstration of a curveball since wind can also produce a curved trajectory. The effects of wind can be avoided by experimenting in a gym.

D. Comparison of simulated and measured curveball trajectories

The normal and inverse Magnus effects can be modeled using positive and negative lift coefficients in Eq. (39), respectively. Figures 10 and 11 illustrate curveballs for a soccer ball and a plastic ball shot with the same orientation of the spin vector (positive ω_y). The lift coefficients are $c_L = 0.9$ for the soccer ball and $c_L = -0.7$ for the smooth plastic ball. The initial conditions are summarized in Table III. The vertical (x, y)-plane shows the shortened trajectory as compared to the vacuum solution. The horizontal (x, z)-plane reveals the curve that a spinning ball follows in air. The vacuum trajectory is a straight line in the (x, z)-plane from which the spinning ball deviates substantially. The soccer ball curves the right way as is expected from sports balls.

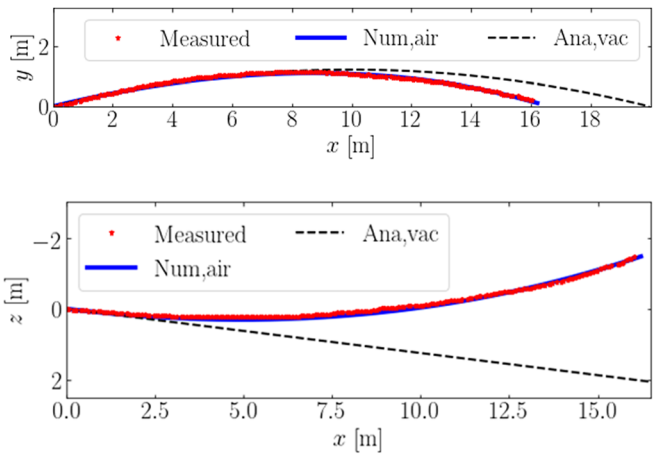

Fig. 10. Trajectory of a soccer ball with spin. Comparison between predicted and measured trajectory. Recall that the y-axis is vertical, and the z-axis is horizontal.

However, the plastic ball, which was shot with the same orientation of the spin vector as the soccer ball, curves the wrong way compared to the expectation that we have for sports balls. In both cases, the measured and simulated trajectories accounting for air drag are in very good agreement. The cell phone camera was positioned at $z = 0$. The curveball trajectory causes that z changes sign at some point on the trajectory when the ball crosses the direct line from the camera to the soccer player.

E. Comparison of simulated and experimental trajectories of balls with topspin and backspin

Curveballs curve due to the effect of sidespin on the ball. It is easy to observe this effect for example in soccer since the Magnus force is the only sideways force. For sidespin, it is perpendicular to gravity and to the drag force. Often topspin or backspin is imparted to the ball, for example, in tennis or volleyball. In that case, the Magnus force is somewhat

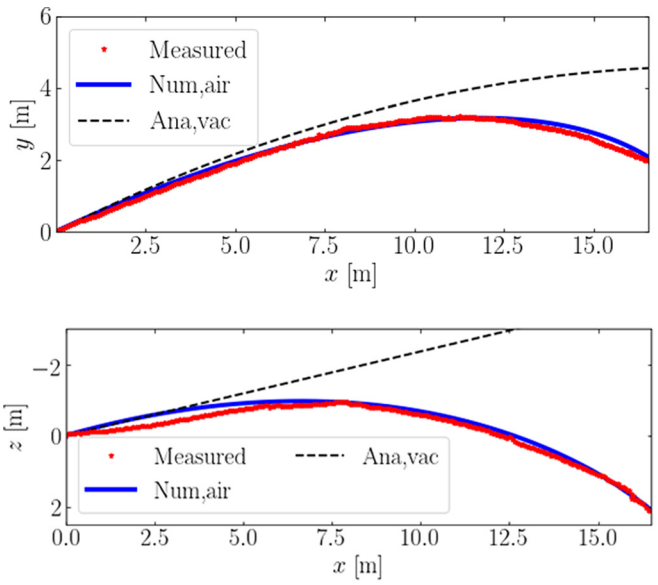

Fig. 11. Trajectory of a plastic ball with spin. Comparison between predicted and measured trajectory. Recall that the y-axis is vertical, and the z-axis is horizontal.

Table III. Spinning ball parameters. Initial conditions, rotations per second (rps), and spin parameters for the soccer ball and the plastic ball.

	v_{x0} (m/s)	v_{y0}(m/s)	v_{z0}(m/s)	ω_{y0}(1/s)	rps	S
Soccer ball	20.0	4.9	2.5	46	7.3	0.24
Plastic ball	21.0	9.8	−6.0	28	4.5	0.13

more difficult to observe and grasp intuitively, since it is in the plane defined by the gravitational force and drag force vectors. The modified trajectory due to topspin or backspin can be studied for tennis or table tennis balls or volleyballs using the same methods as for curveballs. However, the effect is less clearly directly observable.

For the sake of illustration, we now make an exception to our goal to demonstrate low-cost experiments that can be performed by students with their own equipment. Here, we will study simulated and measured trajectories of volleyballs with various backspin and topspin rates but with the same launch speed and launch angle. The spinning volleyballs are delivered by a ball launch machine with adjustable spin rate which is used in top level volleyball training. Humans are usually not capable to just vary the spin rate while keeping the launch angle and the speed constant. In the ball launch machine, two spinning wheels accelerate the volleyball quickly to the launch speed. As the two wheels can be spun at different spin rates, spin can be imparted to the volleyball. The launch angle is kept constant by fixing the orientation of the machine. The launch speed is kept constant by assuring that the sum of the magnitudes of the spin rates of the two wheels is constant during the experiment (Fig. 12).

Figure 13 shows a comparison of the trajectories of volleyballs with various rates of topspin and backspin which are described by the number of rotations per seconds (rps). We also plot a vacuum trajectory for reference. The larger the topspin, the larger the downward Magnus force and the faster the ball dips below the trajectory of the ball without spin. The larger the backspin, the stronger the upward Magnus force and the longer the range of the ball becomes. For backspin, the Magnus force becomes a lift force opposing gravity, as for an aircraft wing. In this experiment, the range of the ball delivered with backspin remains shorter than the theoretical vacuum range. However, trajectories of balls with backspin always achieve a larger height on some part of the trajectory due to the lift force.

Comparing the measured and simulated trajectories, we generally find agreement within about one meter and often

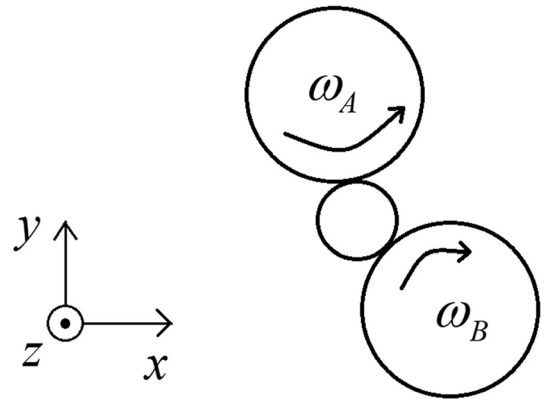

Fig. 12. Illustration of the ball launch machine. Varying the spin rate at constant launch speed is achieved by the condition $|\omega_A| + |\omega_B| =$ constant.

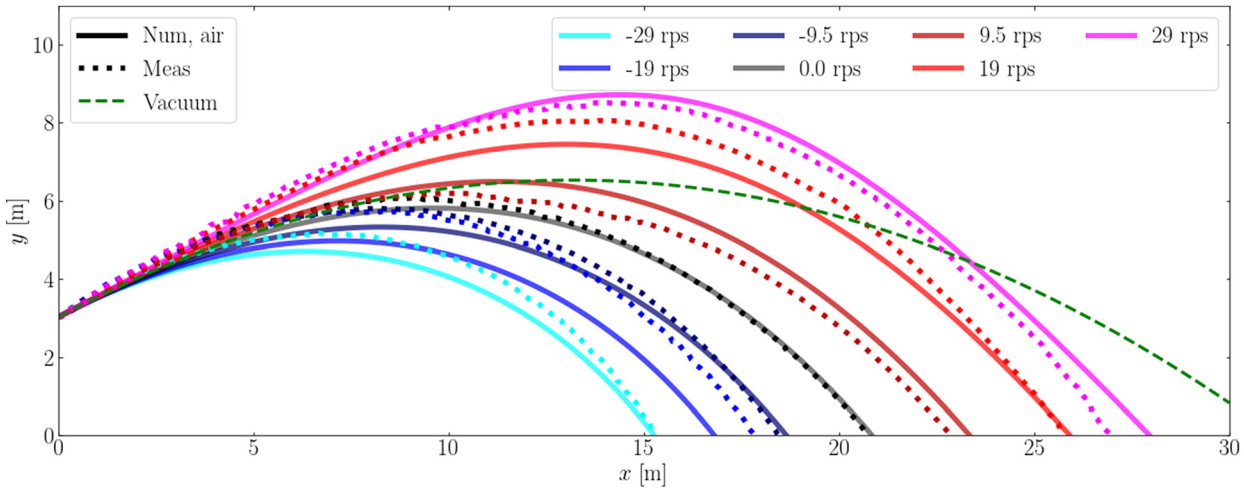

Fig. 13. Comparison between predicted and measured trajectories of balls delivered with a ball machine capable of delivering topspin and backspin. The launch velocity vector is the same for each launch ($v_{x0} = 15.6$ m/s, $v_{y0} = 8.3$ m/s), while the rotation rate is varied. Topspin has a negative sign (blue color tones), and backspin has a positive sign (red color tones). The spin parameters S are 0, ± 0.36, ± 0.71, and ± 1.07. A trained volleyball player may achieve $S \sim -0.2$.

less. The volleyball is well described by the drag model for c_D in Eq. (23) with the parameters $v_c = 19.7$ m/s and $v_s = 11.9$ m/s as well as a lift force coefficient $c_L = 0.175$. The launch of the volleyballs was filmed close-up so that measurements of the spin rates and launch velocity are available. The launch velocity components were $v_{x0} = 15.6$ m/s and $v_{y0} = 8.3$ m/s. The different spin parameters are given in the caption of Fig. 13. The level of agreement varies for the different shots. The agreement is best for the case without spin throughout the whole trajectory. Discrepancies between the measured and simulated trajectories most likely originate from inaccurate measurements of the initial conditions and inaccurate tracking of the ball. Furthermore, the models for the drag and lift coefficients c_D and c_L may not be good for such large spin rates. A spin parameter $S > 1$ (here > 27 rps) even means that locally, close to the equator, the surface moves in the opposite direction of the center-of-mass of the ball. Nevertheless, overall agreement is satisfactory for our purpose.

IV. BOUNCING OF SPINNING BALLS

A. Theoretical bounce model

The bounce of the ball can be calculated using the linear and angular impulse-momentum theorems along with coefficients of restitution for the ball-surface pair in the vertical and horizontal directions.[28–31] The linear impulse-momentum theorem is obtained by integrating Newton's second law in time,

$$\int \sum \mathbf{F} dt = m\mathbf{v}_2 - m\mathbf{v}_1. \tag{50}$$

Likewise, the angular impulse-momentum theorem is

$$\int \sum \mathbf{R} \times \mathbf{F} dt = I\boldsymbol{\omega}_2 - I\boldsymbol{\omega}_1. \tag{51}$$

$\mathbf{R}$ is the vector from the center of the ball to the contact point (Fig. 14). I is the moment of inertia, which for a ball with radius R is

$$I = \alpha m R^2. \tag{52}$$

For hollow balls, as most sports balls, $\alpha = 2/3$. For solid balls, such as billiard balls, $\alpha = 2/5$.

We now calculate the velocity and spin vectors after the bounce from the velocity and spin vectors before the bounce. We assume that $\mathbf{R}$ is constant during the bounce such that we can pull it out of the integral. This neglects the deformation of the ball during the bounce which we can assume to be fairly small compared with the radius, i.e., we assume a contact point rather than a contact area. Eliminating the unknown impulse $\int \sum \mathbf{F} dt$ gives

$$\mathbf{R} \times (m\mathbf{v}_2 - m\mathbf{v}_1) = I\boldsymbol{\omega}_2 - I\boldsymbol{\omega}_1. \tag{53}$$

As this vector equation represents three equations with six unknowns (the components of $\boldsymbol{v}_2$ and $\boldsymbol{\omega}_2$), we need three extra equations. An often used concept is the coefficient of restitution which describes how much energy is converted into sound and heat during the bounce. The vertical coefficient of restitution is defined as

$$e_y = -\frac{v_{y,2}}{v_{y,1}}. \tag{54}$$

We have $e_y \in [0; 1]$. $e_y = 1$ corresponds to a perfectly elastic bounce with no conversion of kinetic energy into sound and heat. $e_y = 0$ corresponds to a perfectly inelastic collision after which the ball just lies flat on the ground and does not rebound at all, as for example, a sandbag. The horizontal coefficients of restitution are defined as[31]

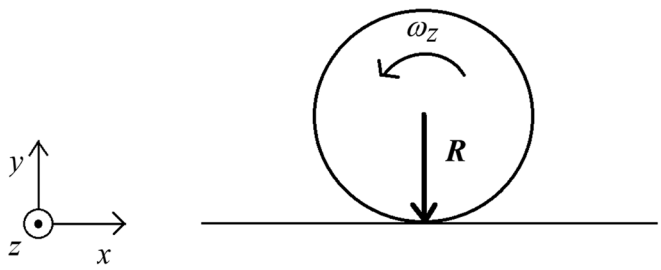

Fig. 14. Geometry and coordinates for the bounce of a ball.

$$e_x = -\frac{v_{x,2} + R\omega_{z,2}}{v_{x,1} + R\omega_{z,1}}, \tag{55}$$

$$e_z = -\frac{v_{z,2} - R\omega_{x,2}}{v_{z,1} - R\omega_{x,1}}. \tag{56}$$

In the definition of e_y, the vertical velocity components of the center-of-mass right before and after the bounce are used (which are identical to those of the contact point). However, for horizontal coefficients of restitution, the horizontal velocity components of the contact point are used. Usually, $e_x = e_z$ because coefficients of restitution are parameters characterizing the pair of materials of the ball and the surface, and usually no difference is expected for the two horizontal directions. We have $e_{x,z} \in [-1; 1]$. A perfectly elastic collision in the horizontal direction reverses the horizontal velocity of the contact point which happens for $e_{x,z} = 1$. Smaller positive $e_{x,z}$ still reverse the direction of the horizontal velocity of the contact point, but to a smaller magnitude. A perfect no-slip condition in the two horizontal directions is described by the conditions $v_{x,2} = -R\omega_{z,2}$ and $v_{z,2} = R\omega_{x,2}$ which corresponds to $e_{x,z} = 0$. (The no-slip condition also describes an idealized rolling ball with no slip.) Gliding with friction corresponds to a horizontal slowing down of the impact point which occurs for negative $e_{x,z}$. Frictionless gliding corresponds to $e_{x,z} = -1$.

Solving the six equations for the unknown velocities and spin rates after the bounce, we get

$$v_{x,2} = \frac{1 - \alpha e_x}{\alpha + 1} v_{x,1} - \frac{\alpha(1 + e_x)}{\alpha + 1} R\omega_{z,1}, \tag{57}$$

$$v_{y,2} = -e_y v_{y,1}, \tag{58}$$

$$v_{z,2} = \frac{1 - \alpha e_z}{\alpha + 1} v_{z,1} + \frac{\alpha(e_z + 1)}{\alpha + 1} R\omega_{x,1}, \tag{59}$$

$$\omega_{x,2} = \frac{\alpha - e_z}{\alpha + 1} \omega_{x,1} + \frac{e_z + 1}{\alpha + 1} \frac{v_{z,1}}{R}, \tag{60}$$

$$\omega_{y,2} = \omega_{y,1}, \tag{61}$$

$$\omega_{z,2} = \frac{\alpha - e_x}{\alpha + 1} \omega_{z,1} - \frac{e_x + 1}{\alpha + 1} \frac{v_{x,1}}{R}. \tag{62}$$

Note that $v_{x,2}$ depends only on $v_{x,1}$ and $\omega_{z,1}$, and that $v_{z,2}$ depends only on $v_{z,1}$ and $\omega_{x,1}$. Similarly, $\omega_{x,2}$ depends only on $\omega_{x,1}$ and $v_{z,1}$, and $\omega_{z,2}$ depends only on $\omega_{z,1}$ and $v_{x,1}$. The y-direction is decoupled: v_y reverses the direction and decreases in magnitude. ω_y is constant over the bounce since we have assumed a contact point such that the friction forces during the bounce provide no torque in the vertical direction y. We can further see that if the ball is in the no-slip condition $v = \pm R\omega$, then v and ω are constant over the bounce.

The bounce equations can be conveniently written as a matrix equation,

$$\begin{pmatrix} v_{x,2} \\ v_{y,2} \\ v_{z,2} \\ \omega_{x,2} \\ \omega_{y,2} \\ \omega_{z,2} \end{pmatrix} = \mathbf{B} \begin{pmatrix} v_{x,1} \\ v_{y,1} \\ v_{z,1} \\ \omega_{x,1} \\ \omega_{y,1} \\ \omega_{z,1} \end{pmatrix}, \tag{63}$$

where $\mathbf{B}$ is the bounce matrix,

$$\mathbf{B} = \begin{pmatrix} \frac{1-\alpha e_x}{\alpha+1} & 0 & 0 & 0 & 0 & -\frac{\alpha(1+e_x)}{\alpha+1}R \\ 0 & -e_y & 0 & 0 & 0 & 0 \\ 0 & 0 & \frac{1-\alpha e_z}{\alpha+1} & \frac{\alpha(e_z+1)}{\alpha+1}R & 0 & 0 \\ 0 & 0 & \frac{e_z+1}{\alpha+1}\frac{1}{R} & \frac{\alpha-e_z}{\alpha+1} & 0 & 0 \\ 0 & 0 & 0 & 0 & 1 & 0 \\ -\frac{e_x+1}{\alpha+1}\frac{1}{R} & 0 & 0 & 0 & 0 & \frac{\alpha-e_x}{\alpha+1} \end{pmatrix}. \tag{64}$$

An interesting question is what the velocity and the spin vectors of the ball are after N bounces. For each bounce, we multiply the velocity and spin vector before the collision with the bounce matrix. For N bounces, we must therefore multiply the initial vector with the bounce matrix to the power of N. To do this, we find the eigendecomposition of the bounce matrix: $\mathbf{B} = \mathbf{Q}\mathbf{\Lambda}\mathbf{Q}^{-1}$, where $\mathbf{\Lambda}$ is a diagonal matrix holding the eigenvalues and the columns of $\mathbf{Q}$ hold the eigenvectors of $\mathbf{B}$. For the bounce matrix, we get

$$\mathbf{\Lambda} = \begin{bmatrix} -e_x & 0 & 0 & 0 & 0 & 0 \\ 0 & -e_y & 0 & 0 & 0 & 0 \\ 0 & 0 & -e_z & 0 & 0 & 0 \\ 0 & 0 & 0 & 1 & 0 & 0 \\ 0 & 0 & 0 & 0 & 1 & 0 \\ 0 & 0 & 0 & 0 & 0 & 1 \end{bmatrix} \tag{65}$$

and

$$\mathbf{Q} = \begin{bmatrix} \alpha R & 0 & 0 & 0 & 0 & -R \\ 0 & 1 & 0 & 0 & 0 & 0 \\ 0 & 0 & -\alpha R & R & 0 & 0 \\ 0 & 0 & 1 & 1 & 0 & 0 \\ 0 & 0 & 0 & 0 & 1 & 0 \\ 1 & 0 & 0 & 0 & 0 & 1 \end{bmatrix}. \tag{66}$$

The Nth power of $\mathbf{B}$ is

$$\mathbf{B}^N = \mathbf{Q}\mathbf{\Lambda}^N\mathbf{Q}^{-1}. \tag{67}$$

Then, we obtain a bounce matrix for N bounces,

$$\mathbf{B}^N = \mathbf{Q} \begin{bmatrix} (-e_x)^N & 0 & 0 & 0 & 0 & 0 \\ 0 & (-e_y)^N & 0 & 0 & 0 & 0 \\ 0 & 0 & (-e_z)^N & 0 & 0 & 0 \\ 0 & 0 & 0 & 1 & 0 & 0 \\ 0 & 0 & 0 & 0 & 1 & 0 \\ 0 & 0 & 0 & 0 & 0 & 1 \end{bmatrix} \mathbf{Q}^{-1}. \tag{68}$$

The velocity and rotation of the ball approach a limit for many bounces, which we find by letting $N \to \infty$. Then, the elements in $\mathbf{\Lambda}$ containing e_x, e_y, or e_z approach zero for any real ball. Thus, the final conditions of a ball bouncing sufficiently many times actually do not depend on the coefficients

of restitution in this idealized model. The coefficients of restitution determine, however, how fast the ball converges to these limits: The smaller $|e_{x,y,z}|$, the faster the convergence towards the limit. In the limit $N \to \infty$, we obtain

$$\lim_{N\to\infty} \mathbf{B}^N = \begin{bmatrix} \frac{1}{1+\alpha} & 0 & 0 & 0 & 0 & \frac{-\alpha}{1+\alpha}R \\ 0 & 0 & 0 & 0 & 0 & 0 \\ 0 & 0 & \frac{1}{1+\alpha} & \frac{\alpha}{1+\alpha}R & 0 & 0 \\ 0 & 0 & \frac{1}{1+\alpha}\frac{1}{R} & \frac{\alpha}{1+\alpha} & 0 & 0 \\ 0 & 0 & 0 & 0 & 1 & 0 \\ \frac{-1}{1+\alpha}\frac{1}{R} & 0 & 0 & 0 & 0 & \frac{\alpha}{1+\alpha} \end{bmatrix}. \tag{69}$$

The velocity in the y-direction goes towards zero, corresponding to the conversion of kinetic energy into sound and heat during each bounce. The spin in the y-direction is constant. The only difference between the first and the last row is a factor of $-R$. Similarly, the only difference between the third and the fourth row is a factor R. Writing out the x and z-components explicitly shows the relation between the initial conditions and the final conditions after many bounces,

$$v_{x,N\to\infty} = \frac{1}{1+\alpha} v_{x,1} - \frac{\alpha R}{1+\alpha}\omega_{z,1}, \tag{70}$$

$$v_{z,N\to\infty} = \frac{1}{1+\alpha} v_{z,1} + \frac{\alpha R}{1+\alpha}\omega_{x,1}, \tag{71}$$

$$\omega_{x,N\to\infty} = \frac{1}{1+\alpha}\frac{1}{R} v_{z,1} + \frac{\alpha}{1+\alpha}\omega_{x,1}, \tag{72}$$

$$\omega_{z,N\to\infty} = -\frac{1}{1+\alpha}\frac{1}{R} v_{x,1} + \frac{\alpha}{1+\alpha}\omega_{z,1}. \tag{73}$$

This limit implies that balls will approach the no-slip condition after a sufficiently large number of bounces if $|e_{x,z}| < 1$,

$$v_{x,N\to\infty} = -\omega_{z,N\to\infty} R, \tag{74}$$

$$v_{z,N\to\infty} = \omega_{x,N\to\infty} R. \tag{75}$$

For $e_{x,z} = -1$, we have pure gliding and $v_{x,z}$ and $\omega_{x,z}$ do not change. For $e_{x,z} = 1$, the velocity and the angular frequency will reverse the velocity of the contact point for each bounce. The balance between the translational and the rotational terms determines in which direction the ball ends up bouncing in each case. Note that the limit $N \to \infty$ describes the motion of the ball after many bounces, but not the transition to actual rolling which happens when the ball does not detach from the ground any more. This leads to the preservation of vertical spin ω_y during many bounces if the contact area between the ball and the surface is modeled as a point. To model the disappearance of vertical spin, the finite size of the contact area must be accounted for, rather than assuming a contact point. Friction on the contact area provides a torque against the direction of vertical spin. Codes solving these equations are provided in the supplementary material.[32]

B. Comparison of theoretical and experimental trajectories of bouncing balls

In this subsection, we compare the computed results using the bounce equations with experimental data. For each ball, we track the motion of the ball for three to four bounces using the same experimental methods as for spinning balls in flight. A bouncing soccer ball is tracked on dry and on wet grass. The basketball is tracked on a basketball court. Finally, a superball on wood is also tracked. As the speeds of the balls in these experiments are quite low, the ballistic parameters are high, and we can use the analytic vacuum trajectories for the flight phases. Here, we release the ball in the (x, y)-plane and impart backspin in the z-direction. The initial conditions of our bounce experiments are summarized in Table IV.

First, we find the vertical and horizontal coefficients of restitution which are assumed to be independent. The vertical coefficient of restitution is most reliably found from the trajectory heights before and after the bounce, H_1 and H_2. Neglecting air drag, we get

$$e_y = -\frac{v_{y,2}}{v_{y,1}} = \sqrt{\frac{H_2}{H_1}}. \tag{76}$$

The horizontal coefficients of restitution are found by fitting the theoretical model for the bounce to the experimental data. In each case, we present several bounces which are well described by a single horizontal and a single vertical coefficient of restitution. Once these two coefficients of restitution are found experimentally for a given ball-surface pair, they can be used to predict the motion of a bouncing ball for other velocities and spin rates before the bounce. Within the typical speed and spin rates of balls in sports, this model gives a good match to the experimental data (Fig. 15).

The measured coefficients of restitution are summarized in Table IV. For the soccer ball on wet and dry grass, the vertical coefficient of restitution is about 0.6 whereas, for a basketball and the superball, it is larger than 0.8. Much larger differences are found for the horizontal coefficient of restitution which reflects the different impact regimes: frictionless gliding ($e_{x,z} = -1$), gliding with friction ($e_{x,z} < 0$), perfect no-slip collision ($e_{x,z} = 0$), elastic collisions ($e_{x,z} > 0$), and perfectly elastic collisions ($e_{x,z} = 1$). The soccer ball on wet grass glides through the impact with little friction ($e_{x,z} = -0.75$). The soccer ball on dry grass and the basketball are quite close to the no-slip model on the elastic rather than the gliding side ($e_{x,z} \sim 0.1$). A superball is close to a perfectly elastic collision ($e_{x,z} = 0.83$). Due to this very high horizontal coefficient of restitution, the superball reverses the direction and the spin vector during all tracked bounces, i.e., it is the only ball that bounces back and forth. The soccer ball and the basketball are released with backspin. They reverse the direction only in the first bounce and then continue bouncing in the same direction (Fig. 15).

V. DISCUSSION AND CONCLUSIONS

In a three-day project in high school or the first year of university, the students compute and measure trajectories of

Table IV. Initial conditions and horizontal and vertical coefficients of restitution for the different bouncing balls.

	v_{x0}(m/s)	v_{y0}(m/s)	ω_{z0}(1/s)	$e_{x,z}$	e_y
Soccer ball (no spin, wet)	−5.5	−5	0	−0.75	0.57
Soccer ball (spin, dry)	−1.7	−8	−32.8	0.12	0.62
Basketball	−1.55	−8	−30	0.1	0.825
Superball	−0.85	−3.95	−49	0.83	0.825

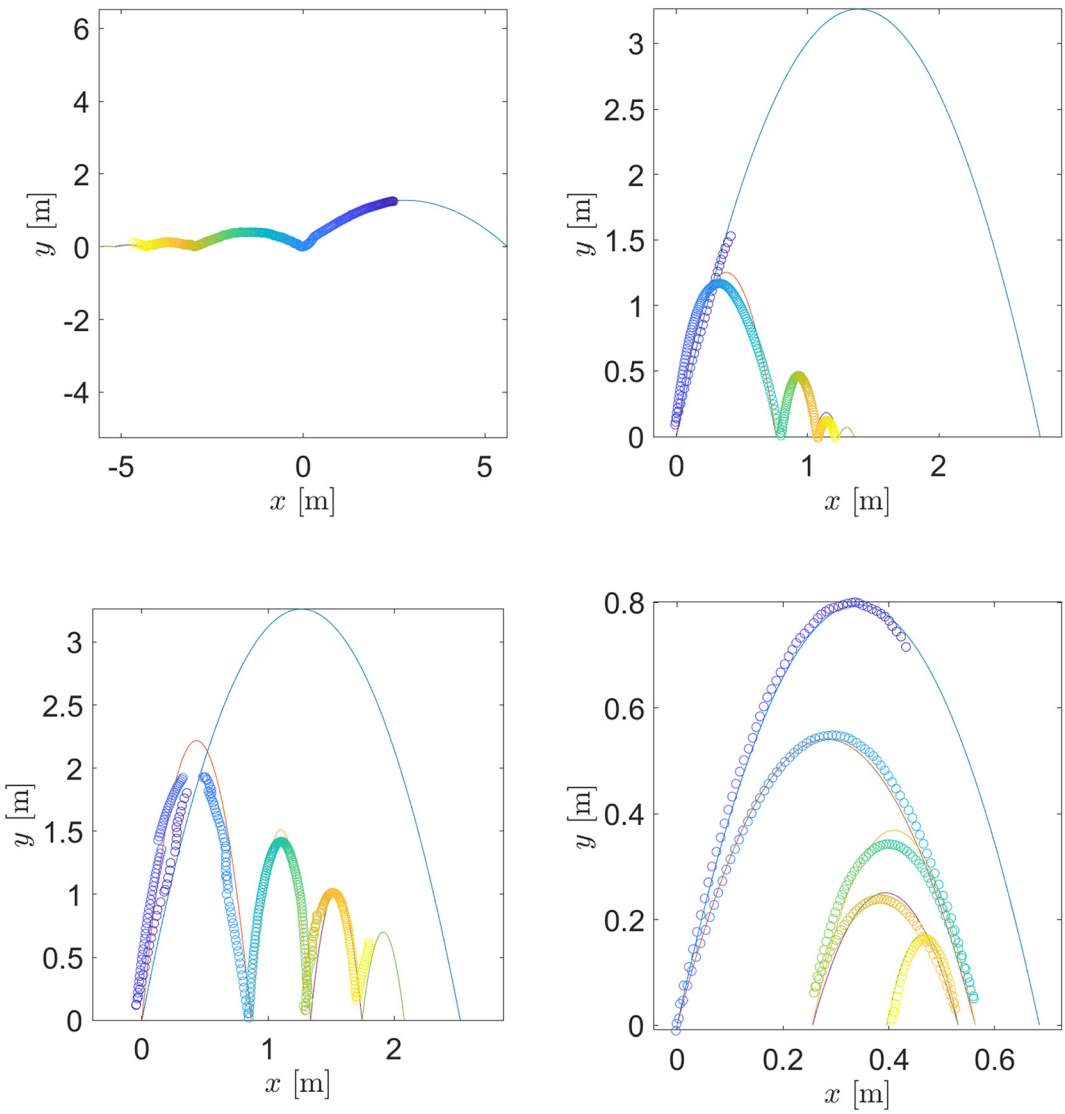

Fig. 15. Comparison between predicted (solid lines) and measured (circles) trajectories of bouncing balls. Top left: Soccer ball (wet, no spin); top right: Soccer ball (dry, backspin); bottom left: Basketball with backspin, bottom right: Superball with backspin. The colors of the measurements illustrate the advancement of time from blue to yellow.

balls in flight and of bouncing balls. These are the most important elements of ball motion in many sports, which provides a strong incentive for many students to study the underlying physics: projectile motion, aerodynamics, collisions, and friction. The comparison of the predictions and the measurements encompasses an illustration of the scientific method of comparing theoretical and computational predictions with experiment. The students' own cell phone cameras have nowadays sufficient frame rates to capture the trajectories and even the spin of many sports balls. As students typically also possess balls in sufficient numbers, the experiments can be performed at little costs for the university. The use of their own equipment tends to motivate the students, too.

We have shown how to obtain trajectories of sports balls by analytic, numerical, and experimental means. In a first step, the trajectories of a shot put, a soccer ball, and a table tennis ball can be compared with analytic vacuum solutions. The experimental shot put trajectory is described by vacuum trajectories to within a few centimeters, but the experimental soccer ball and table tennis ball trajectories are substantially shorter than the corresponding vacuum trajectories. This is explained by the ratio of gravitational and aerodynamic forces, i.e., the ballistic parameter. Numerically computed trajectories accounting for air drag match the measured trajectories very well in all cases. Numerically computed vacuum trajectories can further be benchmarked against the analytically computed vacuum trajectory to illustrate the accuracy of the numerical approach and to obtain an idea of the required time step size.

The trajectories of curveballs and balls with topspin and backspin present a further fascinating meeting ground between theory and observation. Properly designed sports balls curve in the same sense as the ball rotates: The trajectory of a ball with clockwise rotation will curve clockwise, and the trajectory of a ball with anti-clockwise rotation will curve anti-clockwise. However, plastic balls with no surface roughness elements curve the wrong way for a usual kick. Both phenomena can be modeled by the Magnus force, where the Magnus lift coefficients are positive for properly designed sports balls, but negative for smooth plastic balls. Computed and measured curveball trajectories match within

centimeters. We have also shown the effect of topspin and backspin on balls using a ball launch machine. For balls with topspin, the Magnus force has a downward component, and for balls with backspin, it has an upward component. These effects are more difficult to distinguish from gravity and to demonstrate intuitively as compared to curveballs. However, experienced athletes can actually tell from the trajectory of a ball if it has topspin or backspin. Nevertheless, simulations and experiments show a good match for balls with topspin and backspin, too.

Finally, we have studied the bounce of arbitrarily spinning balls which can be described by a bounce matrix based on the linear and angular impulse-momentum theorems and vertical and horizontal coefficients of restitution. Our model assumed a single point of contact between the ball and the surface. These theorems imply that balls change their velocity and spin at each bounce to approach the no-slip condition where the horizontal impulse vanishes. Balls with backspin can end up moving in either direction after many bounces, depending on whether the translational or the rotational motion dominates. This end state after many bounces can be computed from the initial state of the ball.

[a]ORCID: 0000-0002-3699-679X.

[1]R. P. Feynman, R. B. Leighton, and M. Sands, *The Feynman Lectures on Physics* (Caltech, Pasadena, 1963), pp. 9-1–9-9.
[2]M. Lisa, *The Physics of Sports* (McGraw-Hill, New York, 2016), pp. xvi–xvii, 80–140.
[3]R. D. Mehta, "Aerodynamics of sports balls," Annu. Rev. Fluid Mech. **17**, 151–189 (1985).
[4]R. D. Mehta, "Sports ball aerodynamics," in *Sport Aerodynamics*, edited by H. Norstrud (Springer, Wien, New York, 2008).
[5]J. E. Goff and M. J. Carre, "Soccer ball lift coefficients via trajectory analysis," Eur. J. Phys. **31**, 775–784 (2010).
[6]J. W. M. Bush, "The aerodynamics of the beautiful game," in *Sports Physics*, edited by C. Clanet (Les Editions de l'Ecole Polytechnique, Paris, 2013), pp. 171–192.
[7]C. Clanet, "Sports ballistics," Annu. Rev. Fluid Mech. **47**, 455–478 (2015).
[8]R. Cross, "Effects of turbulence on the drag force on a golf ball," Eur. J. Phys. **37**, 054001 (2016).
[9]R. Cross and C. Lindsey, "Measurements of drag and lift on smooth balls in flight," Eur. J. Phys. **38**, 044002 (2017).
[10]G. Dupeux, A. L. Goff, D. Quéré, and C. Clanet, "The spinning ball spiral," New J. Phys. **12**, 093004 (2010).
[11]R. Gaal and D. Voss, "This month in physics history, February 6, 1971: Alan Shepard hits a golf ball on the moon," APS News **26**(2) (2017).
[12]H. D. Young and R. A. Freedman, *University Physics with Modern Physics Technology Update*, 13th ed. (Pearson, Essex, 2014), pp. 77–85, 391.
[13]W. Bauer and G. D. Westfall, *University Physics with Modern Physics*, 2nd ed. (McGraw-Hill, New York, 2014), pp. 74–84, 412–413.
[14]N. P. Linthorne, "Optimum release angle in the shot put," J. Sports Sci. **19**(5), 359–372 (2001).
[15]A. Lenz and F. Rappl, "The optimal angle of release in shot put," arXiv:1007.3689v2 (2010).
[16]C. Crowe, M. Sommerfeld, and Y. Tsuji, *Multiphase Flows with Droplets and Particles* (CRC Press, Boca Raton, 1998), pp. 67–99.
[17]M. Salewski and L. Fuchs, "Consistency issues of Lagrangian particle tracking applied to a spray jet in crossflow," Int. J. Multiphase Flow **33**(4), 394–410 (2007).
[18]A. L. Kiratidis and D. B. Leinweber, "An aerodynamic analysis of recent FIFA world cup balls," Eur. J. Phys. **39**, 034001 (2018).
[19]R. Cross, "Aerodynamics in the classroom and at the ball park," Am. J. Phys. **80**, 289–297 (2012).
[20]J. E. Goff, "Trajectory analysis of a soccer ball," Am. J. Phys. **77**, 1020–1027 (2009).
[21]M. R. Maxey and J. J. Riley, "Equation of motion for a small rigid sphere in nonuniform flow," Phys. Fluids **26**(4), 883–889 (1983).
[22]M. Salewski, "LES of jets and sprays injected into crossflow," Ph.D. thesis, Lund University, Lund, 2006.
[23]F. N. M. Brown, *See the Wind Blow* (University of Notre Dame, Indiana, 1971).
[24]D. McLean, *Understanding Aerodynamics* (John Wiley & Sons, West Sussex, 2013), pp. 427–443.
[25]D. McLean, "Aerodynamic lift, part 1: The science," Phys. Teach. **56**(8), 516–520 (2018).
[26]C. T. Crow, D. F. Elger, B. C. Williams, and J. A. Roberson, *Engineering Fluid Mechanics*, 9th ed. (John Wiley & Sons, New Jersey, 2009), pp. 379–381.
[27]P. K. Kundu and I. M. Cohen, *Fluid Mechanics*, 2nd ed. (Academic Press, Orlando, 2002), pp. 328–332.
[28]R. Cross, "The bounce of a ball," Am. J. Phys. **67**, 222–227 (1999).
[29]R. Cross, "Grip-slip behavior of a bouncing ball," Am. J. Phys. **70**, 1093–1102 (2002).
[30]R. Cross, "Measurements of the horizontal coefficient of restitution for a superball and a tennis ball," Am. J. Phys. **70**, 482–489 (2002).
[31]R. Cross, "Bounce of a spinning ball near normal incidence," Am. J. Phys. **73**(10), 914–920 (2005).
[32]See supplementary material at https://doi.org/10.1119/10.0001659 for Matlab and Python scripts that calculate trajectories of spinning balls in flight and the bounce of balls.